Check for updates

Bioelectromagnetics 44:77–89 (2023)

Analysis of global DNA methylation changes in human keratinocytes immediately following exposure to a 900 MHz radiofrequency field

Jody C. Cantu,[1]* Joseph W. Butterworth,[1] Xomalin G. Peralta,[2] Jason A. Payne,[3] and Ibtissam Echchgadda[3]

[1]General Dynamics Information Technology, JBSA Fort Sam, Houston, Texas
[2]National Academy of Sciences NRC Research Associateship, JBSA Fort Sam, Houston, Texas
[3]Air Force Research Laboratory, 711th Human Performance Wing, Airman Systems Directorate, Bioeffects Division, Radio Frequency Bioeffects Branch, JBSA Fort Sam, Houston, Texas

The increasing use of nonionizing radiofrequency electromagnetic fields (RF-EMFs) in a wide range of technologies necessitates studies to further understanding of biological effects from exposures to such forms of electromagnetic fields. While previous studies have described mechanisms for cellular changes occurring following exposure to low-intensity RF-EMFs, the role of molecular epigenetics has not been thoroughly investigated. Specifically unresolved is the effect of RF-EMFs on deoxyribonucleic acid (DNA) methylation, which is a powerful epigenetic process, used by cells to regulate gene expression. DNA methylation is dynamic and can be rapidly triggered in response to external stimuli such as exposure to RF-EMFs. In the present study, we performed a global analysis of DNA methylation patterns in human keratinocytes exposed to 900 MHz RF-EMFs for 1 h at a low dose rate (estimated mean specific absorption rate (SAR) < 10 mW/kg). We used a custom system to allow stable exposure of cell cultures to RF-EMFs under biologically relevant conditions (37 °C, 5% CO_2, 95% humidity). We performed whole genome bisulfite sequencing directly following RF-EMF exposure to examine the immediate changes in DNA methylation patterns and identify early differentially methylated genes in RF-EMF-exposed keratinocytes. By correlating global gene expression to whole genome bisulfite sequencing, we identified six common targets that were both differentially methylated and differentially expressed in response to RF-EMF exposure. The results highlight a potential epigenetic role in the cellular response to RF-EMFs. Particularly, the six identified targets may potentially be developed as epigenetic biomarkers for immediate responses to RF-EMF exposure. Bioelectromagnetics. 44:77–89, 2023. © 2023 Bioelectromagnetics Society. This article has been contributed to by U.S. Government employees and their work is in the public domain in the USA.

Keywords: DNA methylation; epigenetics; keratinocytes; radiofrequency

INTRODUCTION

Epigenetic changes have been implicated as a mechanism behind many of the reported biological effects from exposure to low-dose radiofrequency electromagnetic field (RF-EMF) [Sage and Burgio 2017; Belpomme et al., 2018]. These changes include elevated microribonucleic acid (microRNA) activity [Dasdag et al., 2015a,b], changes in chromatin remodeling [Belyaev et al., 1997; Belyaev et al., 2006, 2009], and histone modification [Wei et al., 1990]. These epigenetic processes play a central role in controlling gene expression. In mammalian cells, deoxyribonucleic acid (DNA) methylation is another, yet powerful epigenetic mechanism that cells use to regulate gene expression. Methylation can occur at any location in a gene; however, the majority of methylated sites are located in short (<4 kB) regions of DNA that contain cytosine-phosphate-guanine (CpG)-rich regions (called CpG islands) or in long domains of repetitive DNA elements

Conflicts of interest: The author declares that there are no conflicts of interest.

*Correspondence to: Jody C. Cantu, General Dynamics Information Technology, JBSA Fort Sam, Houston, TX.
E-mail: jody.cantu.1@us.af.mil

Received for review 14 February 2022; Revised 25 January 2023; Accepted 4 March 2023

DOI:10.1002/bem.22439
Published online 31 March 2023 in Wiley Online Library (wileyonlinelibrary.com).

© 2023 *Bioelectromagnetics* Society. This article has been contributed to by U.S. Government employees and their work is in the public domain in the USA.

[Jones, 2012; Moore et al., 2013; Plongthongkum et al., 2014]. DNA methylation controls gene expression through the addition (hypermethylation) or loss (hypomethylation) of methyl (CH_3) groups on the 5'-carbon of cytosine residues located within CpG dinucleotides. Specifically, hypermethylation is associated with repression of gene expression while hypomethylation is associated with increased gene expression.

DNA methylation is dynamic and known to be rapidly triggered in response to external stimuli, including nonionizing EM fields. The process has been studied with regard to ionizing EM radiation for many years [Whitfield and Billen 1972; Kalinich et al., 1989; Tawa et al., 1998; Kovalchuk et al., 2004; Koturbash et al., 2005; Ma et al., 2010; Kuhmann et al., 2011; Antwih et al., 2013; Miousse et al., 2017]. Specifically, data have shown alterations in the patterns of DNA methylation and changes in the transcription of genes associated with numerous biological processes and pathological states after exposure to ionizing EM radiation. With regard to nonionizing EM radiation, literature has also pointed to altered gene expression following exposure; however, whether similar alterations in DNA methylation patterns occur following exposure to RF-EMFs has not been fully investigated. A recent study by Mokarram et al. [2017] showed that exposure of Sprague Dawley rats to 900 MHz RF-EMFs (SAR 0.95 W/kg) for 4 h induced changes in the methylation status of the estrogen receptor gene compared to nonexposed controls. Moreover, our previous studies in our laboratory examining the effect of 900 MHz RF-EMFs on DNA methylation using qualitative methods (i.e., DNA methylation ELISA-based assays and methylation restriction enzyme digestion) indicated changes in DNA methylation patterns in human keratinocytes following RF-EMFs. Both studies support that exposure to RF-EMF radiation can induce changes in DNA methylation and, thus, reinforce the need for a better evaluation of the RF-EMF-induced effect in DNA methylation status on a global level.

In order to obtain a comprehensive view of the relationship between RF-EMF and epigenetic modifications, we performed a global analysis of DNA methylation patterns in human keratinocytes exposed to continuous wave (CW) 900 MHz RF-EMFs at an electric field (E-field) intensity of 40 V/m (power density [PD] of 0.424 mW/cm^2) for 1 h. We selected an applied PD within the range of the limits for permissible human RF-EMF exposure of 0.2–1.0 mW/cm^2, as established by the Federal Communications Commission (FCC) [Federal Communications Commission, 2019]. Further, human keratinocytes were selected for this study because they are the predominant cells in the skin, which is considered one of the most exposed tissue to external sources of EMFs. The RF-EMF exposures occurred in a biologically controlled, custom-designed setup in which the environmental conditions were maintained at appropriate levels (37 °C, 5% CO_2, 95% humidity). We performed whole-genome bisulfite sequencing (WGBS) directly following exposures to determine the immediate changes in DNA methylation patterns in RF-EMF exposed cells. The results of these studies are significant in defining the ability of RF-EMFs to affect DNA epigenetics and further highlight the role of epigenetic mechanisms in the cellular response to RF-EMFs.

METHODS

Cell Culture

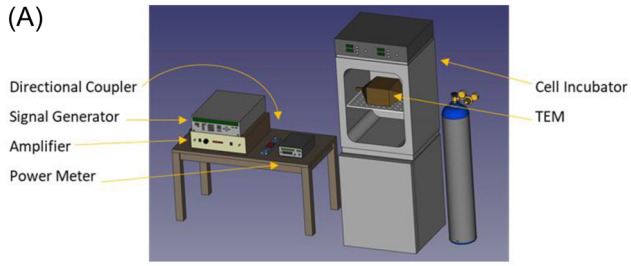
Human epidermal keratinocytes (HEKa) were obtained from ATCC (PCS-200-011, Manassas, VA) and grown in dermal cell basal medium (DMEM) supplemented with 0.4% bovine pituitary extract, 0.5 ng/ml rh TGF-a, 6 mM L-glutamine, 100 ng/ml hydrocortisone hemisuccinate, 5 mg/ml rh Insulin, 1.0 mM epinephrine, 5 mg/ml apo-transferrin, and 10 U/ml Penicillin–Streptomycin–Amphotericin B solution. Cells were incubated at 37 °C with 5% CO_2 in air. The media and its components were purchased from ATCC (Manassas, VA). The cells were maintained by trypsinization once per week and media replacement two times weekly. The day before exposure, cells were plated at a concentration of 20,000 cells/cm^2 on 60 mm tissue-culture treated dishes.

RF Exposure Setup

For all RF-EMF exposures in this study, we used a custom setup that allowed CW 900 MHz RF-EMF exposures of cultured cells in a controlled manner while being maintained at relevant biological conditions (37 °C, 5% CO_2, 95% humidity). In this system, the exposure chamber consisted of a CC-series transverse EM mode cell (TEM Cell, IFI, Ronkonkoma, NY) enclosed in a modified, commercially available incubator (NuAire, Plymouth, MN). The TEM cell was coupled, via an access port on the side wall of the incubator, to a bidirectional coupler (L3Harris Narda-MITEQ, Hauppauge, NY) that was connected to a synthesized RF signal generator (Fluke, Everett, WA) and klystron RF amplifier (Kalmus, Bothell, WA) (Fig. 1A). The access port was sealed with tape to block penetration of outside ambient air. The E-field

1521186x, 2023, 3-4, Downloaded from https://onlinelibrary.wiley.com/doi/10.1002/bem.22439 by University Of British Columbia, Wiley Online Library on [10/10/2026]. See the Terms and Conditions (https://onlinelibrary.wiley.com/terms-and-conditions) on Wiley Online Library for rules of use; OA articles are governed by the applicable Creative Commons License

(A)



(B)

Exposure	Forward Power (W)	E-Field (V/m)	Power Density (mW/cm²)
Sham	0	0	0
Exposed	0.0625	40	0.424

(C)

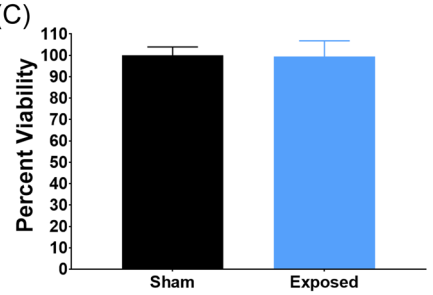


Fig. 1. Experimental setup and characterization of cell exposures at 900 MHz RF-EMF. (**A**) Schematic diagram of the exposure system. Exposures were conducted in a custom, temperature-controlled exposure system (37 °C, 5% CO_2, 95% humidity). (**B**) E-field strength was measured using a NARDA probe for a specific applied forward power. (**C**) Cell viability was profiled during sham and 900 MHz RF-EMF exposure. Percent cell viability was assessed at 24 h following sham or RF-EMF exposure. RF-EMF exposure was compared to sham (that was set to 100%). Data are expressed as percent of the mean value ± SD. The difference in percent viability is not significant (one-way analysis of vaiance). RF-EMF, radiofrequency electromagnetic field.

strength was measured using a Narda isotropic RF electric field probe (L3Harris Narda-MITEQ), and the strength of the input signal was monitored with a power meter (L3Harris Narda-MITEQ). The RF-EMF exposures occurred for 60 min at 40 V/m (0.424 mW/cm^2 PD, Fig. 1B). During exposures, cell culture dishes were placed in the sample holder within the TEM cell. The RF signal was turned ON once the temperature within the incubator was stabilized. For comparison, we performed control (sham) exposures, which consisted of a mock exposure performed similarly without powering on the RF signal. All experimental exposures (RF or sham) were performed on the same system, in randomized, sequential order.

Importantly, the study was performed as a blind experiment. Specifically, the samples were given an ID number and the RF operator was given a chart describing how he should expose the samples (either to RF or sham); therefore, the scientists working with the samples (preparing RNA/DNA, performing viability assays, etc.) were blinded to the identities of the samples. When the samples were submitted to the genetic analysis companies (Genewiz and Epigentek), they were only provided the sample IDs. The samples were only identified when necessary for bioinformatics analysis.

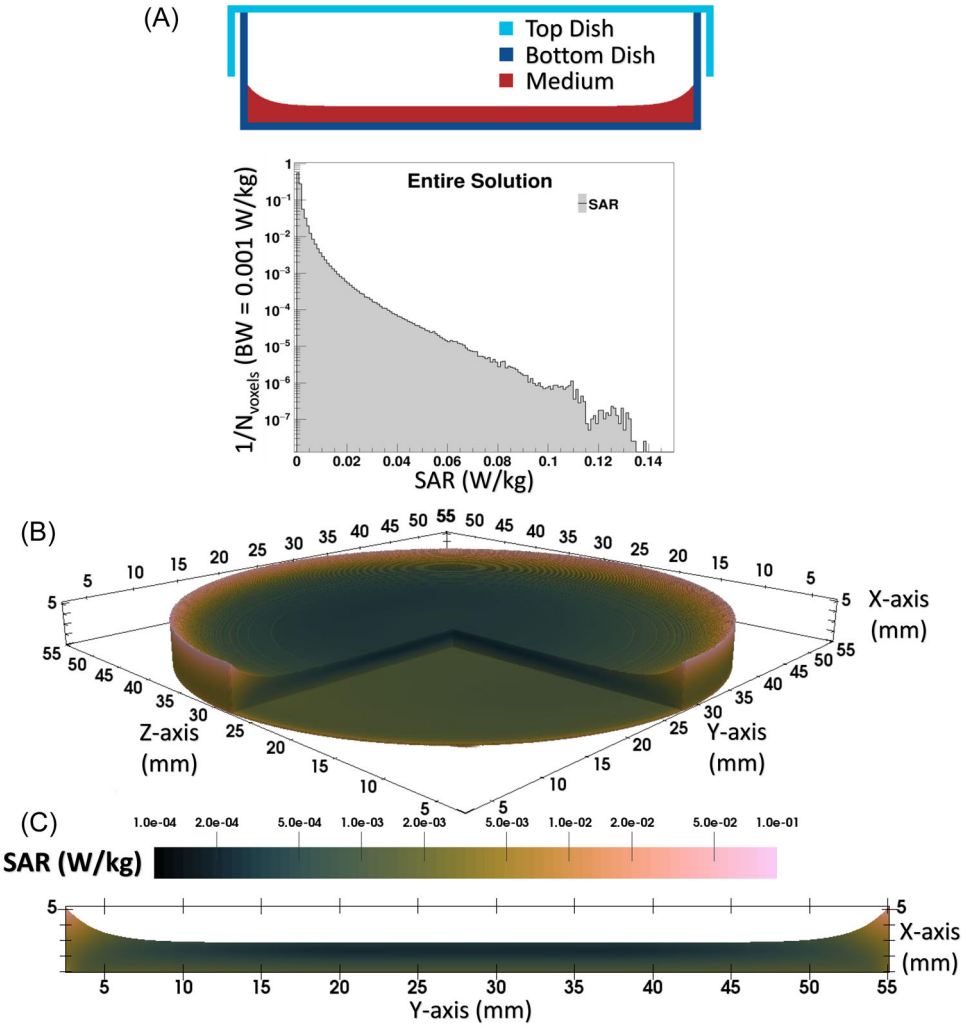
Cell Viability

To evaluate the viability of cells exposed to RF-EMFs compared to sham, MTT (3-(4,5-Dimethylthiazol-2-yl)-2,5-diphenyltetrazolium bromide) Cell Proliferation Assays were conducted. Cell viability was examined 24 h postexposures using MTT assays according to the manufacturer's instructions (ATCC, Manassas, VA). Briefly, exposed cells were incubated for 24 h. Following the incubation period, 500 µl MTT reagent was added, and samples were incubated at 37 °C for 2 h until a precipitate was visible. At this time, 5 ml detergent was added to each well, and the plates were stored in the dark at room temperature overnight. The following day, a 200 µl aliquot of the cell suspension was transferred into a 96-well plate and absorbance was measured at 570 nm with a Synergy HT Plate Reader (BioTek, Winooski, VT).

Dosimetric Modeling of the Exposure System

For the computational dosimetry, we employed Yee finite-difference time-domain (FDTD) modeling techniques to predict the incident fields at the cells while accounting for the 60 mm dish geometry that replicate the empirical exposure conditions [Echchgadda et al., 2016; Remcom, 2020]. Remcom's XFdtd v.7.9 (State College, PA) was used to simulate a 900 MHz plane wave with the E-field polarized in the direction of gravity, incident on the side of a 60 mm dish filled with 5 ml of solution. A grid size was setup with a resolution of 0.05 mm in each direction. A voxelized model of the dish and solution were constructed out of 299 × 1154 x 1154 voxels, where the solution volume was 5.01 ml. The meniscus of the dish and solution interface is described by the NUNC profile presented in Schuderer and Kuster [2003]. Figure 2 represents our modeling of the RF-EMF exposure of cellular medium within the 60 mm cell culture dish geometry, where the plane wave is emitted from the +Z-plane and E-field is polarized along the *X*-axis. Within this simulation, the cell culture dish geometry was modeled by cellular

1521186x, 2023, 3-4, Downloaded from https://onlinelibrary.wiley.com/doi/10.1002/bem.22439 by University Of British Columbia, Wiley Online Library on [10/10/2026]. See the Terms and Conditions (https://onlinelibrary.wiley.com/terms-and-conditions) on Wiley Online Library for rules of use; OA articles are governed by the applicable Creative Commons License



(D)

E-field (V/m)	Bottom Layer		Entire Solution	
	Average SAR (W/kg)	S.D. (W/kg)	Average SAR (W/kg)	S.D. (W/kg)
40	1.55×10^{-3}	7.04×10^{-4}	1.63×10^{-3}	3.11×10^{-3}

Fig. 2. Dosimetric modeling for 900 MHz RF-EMF cell exposures. XFDTD was used to perform RF-EMF exposure dosimetry (Remcom, 2020). (**A**) A medial slice of the voxelized 60-mm Petri dish and 5 ml of cellular medium. (**B**) A histogram of the specific absorption rate (SAR) distribution in the entire cellular medium. The histogram has been normalized by the number of medium voxels (39,692,899 voxels) and the bin width is 0.001 W/kg. (C) Three- and two-dimensional distributions of SAR of the entire solution under RF-EMF exposure. The three-dimensional distribution has a sector of the solution removed, exposing the bottom layer and cross-sections of the SAR distribution. The two-dimensional distribution shows the medial slice in the XY-plane. Both distributions have saturated the upper limit of the SAR color scale. The color map (Crameri, 2021) has been selected to prevent visual distortion of the data and minimize the exclusion of readers with color-vision deficiencies (Crameri et al., 2020). (**D**) Summary of the specific SAR values including the average and standard deviation (SD) SAR values calculated in the bottom 0.15 mm of the solution and in the entire solution. RF-EMF, radiofrequency electromagnetic field.

1521186x, 2023, 3-4, Downloaded from https://onlinelibrary.wiley.com/doi/10.1002/bem.22439 by University Of British Columbia, Wiley Online Library on [10/10/2026]. See the Terms and Conditions (https://onlinelibrary.wiley.com/terms-and-conditions) on Wiley Online Library for rules of use; OA articles are governed by the applicable Creative Commons License

medium (relative permittivity of 71.86 and conductivity of 1.98 S m^{-1}) contained within a polyethylene dish (relative permittivity of 2.55 and conductivity of 4.21 E-05 S m^{-1}) (Fig. 2A). The cellular medium was assumed to be biological saline and the dielectric properties were obtained from Peyman et al. (2007). The polyethylene dish used values from RF Cafe's entry for polystyrene at 900 MHz [Blattenberger, 2022]. The simulation was performed until a steady-state of the electromagnetic fields was reached. The electric field distributions within the cellular medium was used to calculate the specific absorption rate (SAR) values for each voxel,

$$\mathrm{SAR}(r) = \frac{\sigma(r)\,|E(r)|^2}{\rho(r)}, \qquad (1)$$

where r is the voxel index, σ is the electric conductivity, E is the root-mean-square of the steady-state electric field, and ρ is the mass density. Where SAR is proportional to $\sigma(r)\,|E(r)|^2$, the induced current is proportional to $\sigma(r)|E(r)|$. The mean SAR is the mass-weighted average over the voxels of interest,

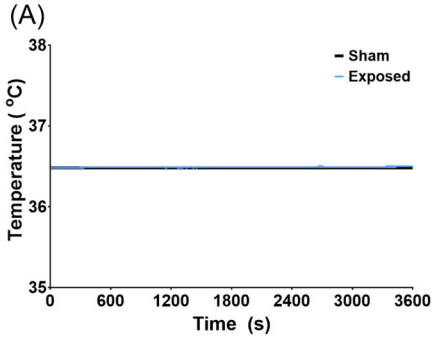
$$\bar{\mathrm{SAR}} = \frac{\sum_i \mathrm{SAR}(r_i)\cdot\rho(r_i)\cdot V(r_i)}{\sum_i \rho(r_i)\cdot V(r_i)}, \qquad (2)$$

where V is the voxel volume. To reduce the impact of numerical artifacts on the curved interfaces with the solution (dish + solution and air + solution), a binary erosion was performed on each horizontal layer of solution voxels. The erosion resulted in the removal of 0.05 ml in the reported SAR values. The mean SAR values were calculated for the solution.

The results of this simulation indicated a mean SAR of 1.63×10^{-3} W/kg in the entire solution during RF-EMF exposure (Figs. 2B and 2C). The mean SAR in a plane at the bottom (0 to 0.15 mm) of the saline (i.e. where the cells are plated) is 1.55×10^{-3} W/kg. A table summarizing the FDTD simulation results is provided in Figure 2D. The largest SAR values are found in the meniscus at the solution and dish interface. The high SAR contribution in the meniscus is expected as the incident E-field is parallel to the meniscus. But at the horizontal center of the dish, the top of the solution has a lower mean SAR (and induced current) than the bottom layer as illustrated in Figure 2. At this exposure frequency, the membrane behaves like a short circuit. The mean (max) induced current in the bottom layer would evoke a membrane potential <10 (40) nV, which is 10,000 lower than biologically significant potentials [Durney et al., 1986].

Temperature Measurements

Empirical temperature profiles during RF-EMF and sham exposures were recorded in real-time using a fiber-optic temperature probe (OpSens, Inc., Quebec, Canada) connected to a desktop personal computer. Temperature measurements were captured every second for the duration of the exposures (Fig. 3A). The change in temperature over the duration of the experiments was computed for sham or exposed and statistical significance was evaluated using unpaired T-test (plotted as mean ± SEM, n.s.). The average temperature change (ΔT, i.e., the



(B)

Exposure	Computational (ΔT, °C)	Empirical (ΔT, °C)
Sham	0	0
Exposed	9.26E-4	9.72E-3

Fig. 3. Thermal profiling of 900 MHz RF-EMF Exposure. (**A**) Temperature profiles from a 60 mm dish exposed to sham and 900 MHz RF-EMF at a low-intensity E-field over the duration of exposure (60 min). Temperatures profiles were measured experimentally using Opsens probes. The change in temperature over the duration of the experiments was computed for sham or exposed and statistical significance was evaluated using unpaired *T*-test (plotted as mean ± SEM, ns). (**B**) Computational and empirical temperature-time data quantified in sham or RF-EMF exposed cells. Data is expressed as ΔT (°C, difference of temperature measured at end and start). Computational data was calculated using XFDTD modeling techniques. RF-EMF, radiofrequency electromagnetic field.

1521186x, 2023, 3-4, Downloaded from https://onlinelibrary.wiley.com/doi/10.1002/bem.22439 by University Of British Columbia, Wiley Online Library on [10/10/2026]. See the Terms and Conditions (https://onlinelibrary.wiley.com/terms-and-conditions) on Wiley Online Library for rules of use; OA articles are governed by the applicable Creative Commons License

difference in temperature values recorded before start of exposure and value recorded at end of exposure) for RF-EMF exposure was not significant ($\Delta T = 0.02$ °C, n.s.).

For computational analysis of temperature measurements, the expected temperature rise was calculated using $\Delta T = \mathrm{SAR} \cdot t / C_h$, where t is the exposure time, 3600 s, and C_h is the specific heat, 4200 J/kg/K. Assuming bulk heating of the solution, SAR is taken to be the mean SAR of the entire solution and gives an expected $\Delta T = 0.0014$ °C. Even considering the 999th permille SAR value (0.039 W/kg) in the solution, the exposure will produce a $\Delta T \sim 0.03$ °C. The computation ignores high-order cooling corrections, such as evaporation. In the SAR distribution, the main source of heating will be at the meniscus and bottom layer, where the cells have been plated on the bottom layer. The asymmetry between the top and bottom of the solution heating pattern could result in natural convection. For a straight cylinder of cellular medium in the 60 mm dish, the convection from a vertical flat plate approximation is taken into consideration. Using Churchill–Chu formulation [Churchill and Chu, 1975], the Rayleigh number (the product of Grashof and Prandtl numbers) has the order of $\Delta T \times \mathrm{L}^3$. Assuming a conservative $\Delta T = 0.01$ °C over the depth of the solution at the horizontal center (2 mm), the Rayleigh number is estimated to be an order of magnitude smaller than the calculations performed in Schuderer et al. [2004]. This suggests the gradient would not be strong enough to initiate mass convection.

Extraction of Genomic DNA

Immediately following sham or RF-EMF exposure, genomic DNA was extracted from HEKa cells using the Qiagen DNeasy Blood & Tissue Kit (Qiagen, Germantown, MD) according to the manufacturer's instructions. We isolated DNA from one, 60 mm dish per experiment condition (exposure or sham), and each was repeated in three independent experiments (final $n = 3$ for the experimental condition). The resulting DNA was treated with RNase to degrade any remaining cellular RNA. DNA was assessed for RNA contamination and integrity with gel electrophoresis and measured for concentration and quality by Nanodrop One Microvolume UV-Vis Spectrophotometer (Thermo Fisher Scientific, Framingham, MA). DNA was stored at −20 °C and used for subsequent analysis.

Whole Genome Bisulfite Sequencing (WGBS)

WGBS was conducted for each exposure condition (sham and RF-EMFs) in triplicate by EpiGentek Group. Briefly, DNA (300 ng DNA input) was digested for 2 h with MSP1 enzyme 20 U/sample at 37 °C followed by 2 h with TaqαI 20 U/sample at 65 °C. The digested DNA size selected with <300 bp DNA fragments (CGI enriched) were collected for bisulfite treatment. DNA fragments were bisulfite treated with the Methylamp DNA Bisulfite Conversion Kit (P-1001, Epigentek, Farmingdale, NY). The conversion efficiency of bisulfite-treated DNA was determined by real-time polymerase chain reaction using two pairs of primers. The first pair (β-actin) amplified bisulfite-converted DNA and the second pair (glyceraldehyde-3-phosphate dehydrogenase) amplified unconverted DNA within the same positive control sample. DNA was shown to be >99% converted. Libraries were prepared with a combination of DNA end polishing and adaptor ligation, library amplification with indexed primers, and library DNA was purified and eluted in 13 µl of water. Library fragment size distribution and quantification was verified on a Bioanalyzer and KAPA Library Quantification. After verification, 20 nM of sample libraries were subjected to next-generation sequencing on an Illumina HiSeq. 4000 (Illumina, San Diego, CA) according to the manufacturer's instructions.

DMR Identification

To determine the differentially methylated regions (DMR) in the RF-EMF samples, Bismark coverage files were imported in R (language for statistical computing and graphics) environment and processed using the bsseq v1.18.0 R package [Hansen et al., 2012]. CpGs, where at least two sample replicates had at minimum 2x in coverage, were kept for further analysis. The *t*-statistics among the sham and RF-EMF samples were calculated using the bsseq::BSmooth.tstat() function with default parameters. DMR were defined as regions with at least three consecutive CpGs with a mean methylation difference of ≥0.05. DMR annotations were performed using the HOMER v4.10.4 Perl suite of tools [Heinz et al., 2010], which allowed identification of specific differentially methylated gene (DMGs) for subsequent analyses.

Extraction of Total RNA and High-Throughput RNA Sequencing

Total RNA was extracted from sham and RF-EMFs exposed HEKa cells ($n = 3$ per condition) using an RNeasy Mini Kit (Qiagen, Germantown, MD) with on-column DNAse I treatment. The concentration of RNA was measured spectrophotometrically using a Nanodrop One Microvolume UV-Vis Spectrophotometer (Thermo Fisher Scientific, Framingham, MA)

1521186x, 2023, 3-4, Downloaded from https://onlinelibrary.wiley.com/doi/10.1002/bem.22439 by University Of British Columbia, Wiley Online Library on [10/10/2026]. See the Terms and Conditions (https://onlinelibrary.wiley.com/terms-and-conditions) on Wiley Online Library for rules of use; OA articles are governed by the applicable Creative Commons License

and the eluted RNA had a 260/280 ratio of > 1.8. The high-throughput RNA sequencing of samples was performed by GENEWIZ (South Plainfield, NJ). RNA was analyzed with the Agilent 2100 BioAnalyzer (Agilent Technologies, Santa Clara, CA) and Qubit assay to validate sample quality and quantity. Following quality control, nine RNA libraries were constructed using NEBNext Ultra RNA Library Prep Kit for Illumina with polyA selection (New England Biolabs, Ipswich, MA) with total RNA and were sequenced with an Illumina HiSeq. 2000 (Illumina, San Diego, CA). Approximately 40–50 million paired-end 150 bp reads were obtained per sample and analyzed with CLC Genomics v.11 (Qiagen, Germantown, MD). Differentially expressed genes (DEGs) were defined as an adjusted *P*-value (P_{adj} or false discovery rate) of ≤ 0.05 and an absolute value of $|\log_2 (\text{fold change})| > 0.379$, which corresponded to a fold change (FC) value of ± 1.3.

Statistics

All RF-EMF exposures alongside with their corresponding sham controls described herein were performed in triplicate (on different days), resulting in three independent experimental replicates per condition ($n = 3$). Depending on the experiment, statistical analysis was performed using either the software indicated above or in R. For DMR identification, hypothesis testing in R was performed using either *t*-tests or χ^2 tests, where indicated.

RESULTS

Identification of DMGs Following RF-EMF Exposure

First, we evaluated the effects of RF-EMF (40 V/m, 0.424 mW/cm^2 PD) exposures on cell viability. Under this exposure condition, we observed a similar cellular viability between RF-EMF exposure and sham condition (Fig. 1C). Next, given that RF-EMF effects have been associated with thermal heating, we determined the temperature profiles during exposure to RF-EMFs or sham. The temperature data in Figure 3, depict the thermal changes measured or modeled during exposure. Results indicated no significant temperature increase during exposure to RF-EMFs under our experimental conditions (Fig. 3). Therefore, our experiments are focused on the immediate epigenetic response following exposure to RF-EMFs in the absence of significant thermal heating.

To assess changes in methylation patterns immediately following RF-EMF exposure, we performed WGBS, which is a method that provides an in-depth detection of changes in DNA methylation across the entire genome. We generated sequencing data to a depth of a minimum of 20× per sample and analyzed the data using the BSmooth algorithm, which allows analysis of low-coverage WGBS data and has been demonstrated to accurately estimate methylation levels at single-base pair resolution by borrowing information from nearby CpGs [Hansen et al., 2012]. Figure 4A shows heatmaps for RF-EMF exposure compared to sham (key is provided in Fig. 4B). The heatmap demonstrates the difference in methylation levels and the significant DMRs in the RF-EMF exposure compared to sham. A full list of DMRs with specific percentage of differential methylation is presented in the Supplementary Material (Supplementary Tables S1-S2). In summary, 842 DMRs were identified in the RF-EMF versus sham comparison, which included 411 hypermethylated loci and 431 hypomethylated loci. We applied cutoffs for statistical significance ($|t\text{-stat}| \geq 3.5$) and identified 114 significant DMGs, of which 48 were hypomethylated DMGs and 66 were hypermethylated DMGs (Fig. 4C). Overall, the data indicate that RF-EMFs could elicit differential DNA methylation throughout the genome.

Identification of DEGs Following RF-EMF Exposure

Since methylation can directly affect gene expression, it was important to examine if the identified DMGs were differentially expressed in the RF-EMF-exposed samples. Therefore, we performed high-throughput RNA sequencing to define DEGs immediately following exposure to RF-EMF under the same conditions. Using a statistical cutoff of a false discovery rate (FDR or P_{adj}) of equal to or less than 0.05 ($P_{adj} \leq 0.05$), we identified 1738 DEGs with the RF-EMF exposure compared to sham (Table 1).

An additional significance cutoff was set for the FC difference to narrow down our list of DEGs to those with a $|FC| \geq 1.3$ ($|\log_2(FC)| \geq 0.379$). After applying this cutoff, we identified 1117 genes that were differentially expressed in RF-EMFs (versus sham) (Table 1). The global distribution of gene expression profiles for the RF-EMF exposed samples compared to sham is represented in volcano plots shown in Figure 5A. In this plot, the level of statistical significance (P_{adj} value) for each gene is plotted against the magnitude of FC in expression relative to sham. The genes located out of the borders of the $P_{adj} \leq 0.05$ and $|FC| \geq 1.3$ lines, indicated by the blue and red dots, were considered to be significant DEGs. Of the 1117 DEGs identified in the RF-EMF exposure group, 495 were significantly downregulated and 622 were significantly upregulated (Fig. 5A).

1521186x, 2023, 3-4, Downloaded from https://onlinelibrary.wiley.com/doi/10.1002/bem.22439 by University Of British Columbia, Wiley Online Library on [10/10/2026]. See the Terms and Conditions (https://onlinelibrary.wiley.com/terms-and-conditions) on Wiley Online Library for rules of use; OA articles are governed by the applicable Creative Commons License

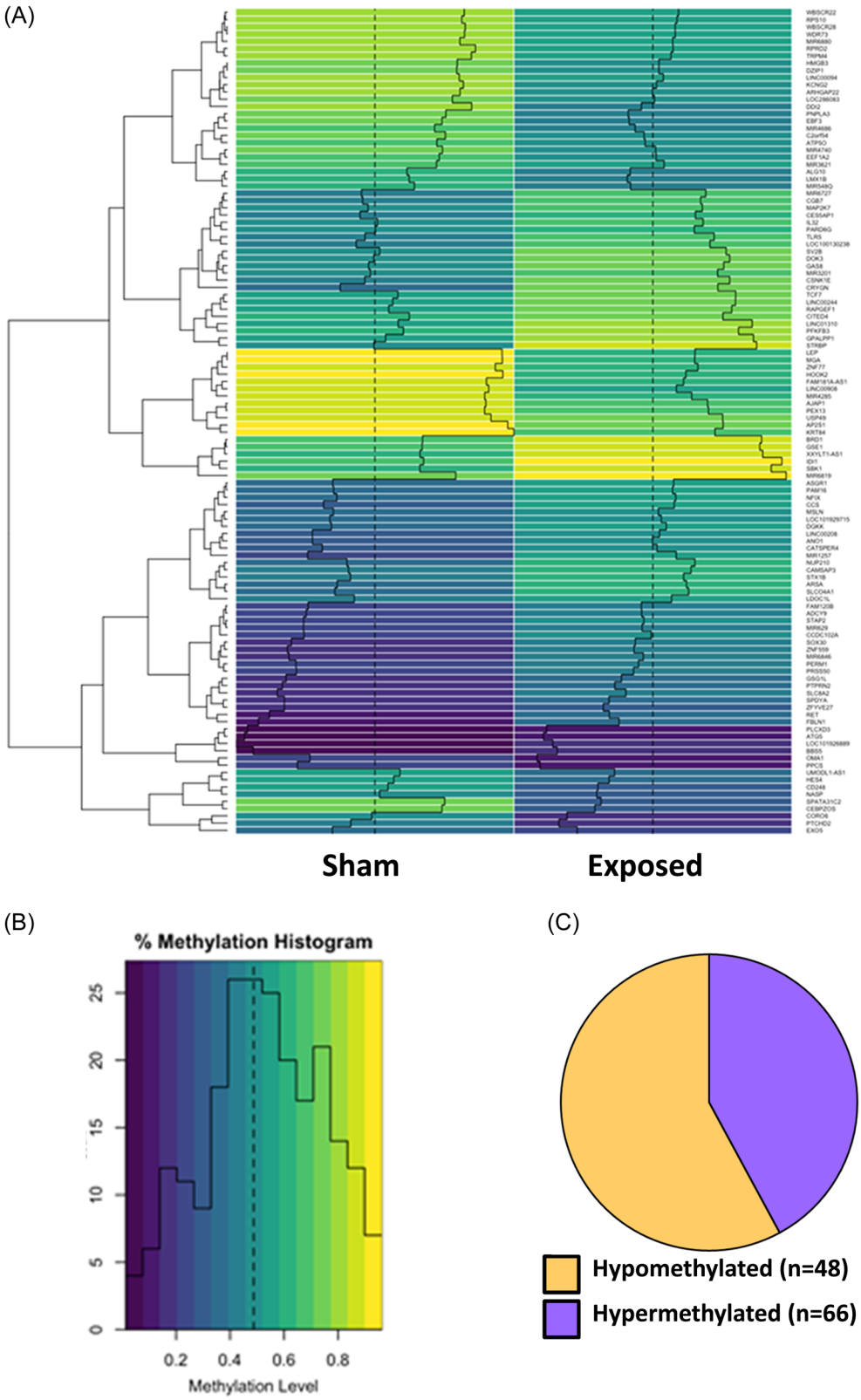


Fig. 4. Continued.

1521186x, 2023, 3-4, Downloaded from https://onlinelibrary.wiley.com/doi/10.1002/bem.22439 by University Of British Columbia, Wiley Online Library on [10/10/2026]. See the Terms and Conditions (https://onlinelibrary.wiley.com/terms-and-conditions) on Wiley Online Library for rules of use; OA articles are governed by the applicable Creative Commons License

TABLE 1. Identification of DEGs Immediately Following Exposure to RF-EMF at Low Intensity E-Fields

Exposure	RF-EMF		
P-value	$P_{adj} \leq 0.05$	1.2FC[a]	1.3FC
Down	743	725	495
Up	995	964	622
Total	1738	1689	1117

[a]Fold change (ratio of one value to another).

Comparison of Gene Expression and DNA Methylation Following RF-EMF Exposure

As mentioned above, modification of DNA methylation patterns can result in alteration of gene expression. Generally, hypermethylation tends to downregulate gene expression and hypomethylation tends to upregulate gene expression. Therefore, we performed a pairwise comparison analysis of the significant DMGs with the significant DEGs within the RF-EMF exposure group to correlate differential DNA methylation with differential gene expression and identify potential overlapping immediate response markers for RF-EMF. The comparison analysis revealed only six genes in the RF-EMF exposure group that had a significant change in both DNA methylation and gene expression (Fig. 5B). These genes are described in Table 2 (gene expression is shown in Supplementary Fig. 1). For the six identified genes, there was an evident positive correlation between DNA methylation and gene expression. As shown in Figure 5C, when the genes were hypermethylated, their expression decreased; contrastingly, when the genes were hypomethylated, their expression was increased. This pairwise comparison results, at least in part, validate that changes in DNA methylation induced by RF-EMFs can elicit changes in gene expression.

DISCUSSION AND CONCLUSION

In a previous study, we used global DNA methylation ELISA-based assays and methylation-sensitive restriction enzyme digestion to investigate the effect of 900 MHz RF-EMFs on DNA methylation. The results, although merely qualitative, indicated the potential of RF-EMFs to alter DNA methylation patterns in human keratinocytes. The present study extended these previous investigations with the goal of gaining a more comprehensive and quantitative view of the immediate effect of RF-EMF exposure and specifically sought to perform a genome-wide analysis of changes in DNA methylation promptly following exposure to RF-EMFs at a low dose. Specifically, the present study examined immediate changes in DNA methylation following 1 h exposure to 900 MHz RF-EMFs at an intensity that did not generate a significant increase in temperature.

Correlation of Gene Expression and DNA Methylation Following RF-EMF Exposure

The results of the present study identified 114 genes that were significantly differentially methylated following exposure to RF-EMFs compared to sham. A correlation to global gene expression revealed six common targets that were both differentially methylated and differentially expressed following in response to RF-EMF exposure (Fig. 5), which could be further studied for potential implication as biomarkers of the epigenetic response to RF-EMF exposure. These genes include targets involved in critical cell functions such as cell survival and response to damage. Specifically, we observe hypomethylation and consequential upregulation of DNA damage inducible 1 homolog 2 (DDI2). DDI2 encodes an aspartyl protease that is involved in the regulation of cell survival following stress by promoting the processing, nuclear translocation, and, thereby, activation of the transcription factors nuclear respiratory factors 1 and 3 (NRF1 and NRF3) [Koizumi et al., 2016; Chowdhury et al., 2017]. NRF1 and NRF3 are key factors controlling the ubiquitin-proteasome system, which mediates the turnover of proteins from a number of biological processes including cell cycle progression, signal transduction, and gene transcription [Hershko, 2005; Chowdhury et al., 2017]. Thus, the upregulation of DDI2 observed following RF-EMF exposure would presumably increase the activity of downstream effectors, including NRF1 and NRF3, which could result in downstream biological effects. Another common gene

Fig. 4. Analysis of DNA methylation patterns in RF-EMF exposed cells. (**A, B**) Hierarchical clustering heatmaps showing the DNA methylation patterns of significant DMRs following RF-EMF exposure (compared to sham). The key for reading the histogram is shown in B and summarized as yellow = 100% methylated and purple = 0% methylated. (**C**) The distribution of differential methylation is shown including the number of hypomethylated or hypermethylated genes in RF-EMF exposure compared to sham. DMGs identified as significantly different in each comparison group (defined as t-stat $\geq$ |3.5|) were classified as hypomethylated or hypermethylated. RF-EMF, radiofrequency electromagnetic field.

1521186x, 2023, 3-4, Downloaded from https://onlinelibrary.wiley.com/doi/10.1002/bem.22439 by University Of British Columbia, Wiley Online Library on [10/10/2026]. See the Terms and Conditions (https://onlinelibrary.wiley.com/terms-and-conditions) on Wiley Online Library for rules of use; OA articles are governed by the applicable Creative Commons License

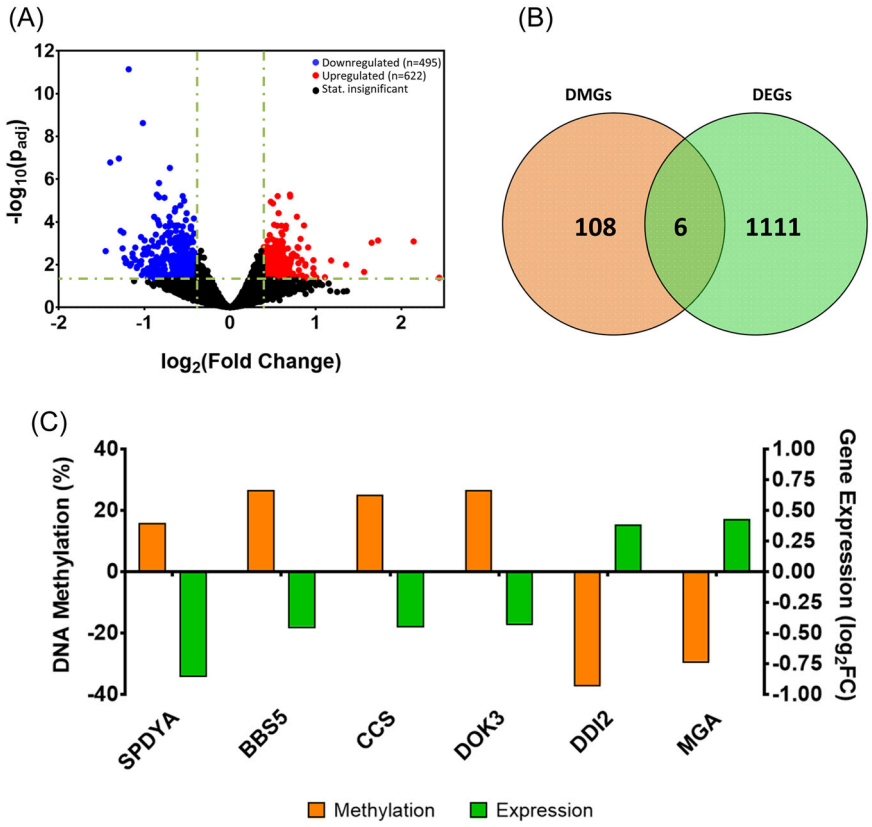


Fig. 5. Comparison of differential DNA methylation and gene expression. (**A**) Differential expression profiles of several genes in RF-EMF exposed cells is highlighted in the Volcano plot. Significance was defined as $P_{adj} \leq 0.05$ with $|FC| \geq 1.3$. Genes highlighted in blue are downregulated and genes in red are upregulated. (**B**) Venn diagram displaying common and unique significant DEGs to DMGs for RF-EMF exposure. (**C**) Correlation between DNA methylation and gene expression for the six genes identified as common in the RF-EMF comparison. All data shown in the graph are statistically significant (DEG $P_{adj} \leq 0.05$ or a DMG $|t\text{-stat}| > 3.5$). Comparisons are relative to sham. RF-EMF, radiofrequency electromagnetic field.

TABLE 2. Correlated Genes from DNA Methylation and Gene Expression Analyses

Gene ID	Description	%Me	$\log_2$FC
SPDYA	Speedy protein A	15.94	−0.846
BBS5	Bardet–Biedl syndrome 5 protein	26.63	−0.447
CCS	Copper Chaperone for superoxide dismutase	24.97	−0.444
DOK3	Docking protein 3	26.63	−0.422
DDI2	DNA damage inducible 1 homolog 2	−36.93	0.387
MGA	MAX dimerization protein MGA	−29.16	0.431

identified as both hypermethylated and downregulated is docking protein 3 (DOK3). DOK3 encodes an important scaffolding protein that provides a docking platform for the assembly of multimolecular signaling complex [Mashima et al., 2009]. Importantly, DOK3 is known to be a negative regulator of c-Jun N-terminal kinase (JNK) [Mashima et al., 2009]. This is important given the role of JNK as a key regulator in apoptosis, where prolonged JNK activation contributes to cell death, including following exposure to ionizing radiation [Tournier et al., 2000; Shaulian and Karin 2002; Liu et al., 2004; Liu and Lin 2005]. Future studies will focus on DDI2, DOK3, and the other four-shared DMGs/DEGs identified in this study to examine the likelihood that these six targets could be biomarkers of RF-EMF exposure and relate the observed genetic and epigenetic changes to downstream biological functions.

Low Dose RF-EMF Induces Genetic Changes in the Absence of Measurable Heating

It is known that, when cells are exposed to stressful stimuli (such as heat) they rapidly elicit a defense mechanism, referred to as the cellular stress

1521186x, 2023, 3-4, Downloaded from https://onlinelibrary.wiley.com/doi/10.1002/bem.22439 by University Of British Columbia, Wiley Online Library on [10/10/2026]. See the Terms and Conditions (https://onlinelibrary.wiley.com/terms-and-conditions) on Wiley Online Library for rules of use; OA articles are governed by the applicable Creative Commons License

response (CSR), to minimize the effects from insults [Kültz 2003, 2005]. CSR involves immediate activation of stress response genes such as those coding for molecular chaperoning, DNA sensing and repair, cell cycle control, and apoptosis [Kültz 2003, 2005]. Thus, given the optimal conditions for living cells in culture required for adequate growth and maintenance is at 37 °C, 95% humidity, and 5% CO_2, it was essential that we conduct all experiments in an environmentally controlled system that allows for these requirements. This controlled system overcomes shortcomings from previous experiments performed in the field, as many studies on the cellular effects of RF-EMFs were conducted at room temperature. Our system combined RF-EMF exposure equipment (i.e., a TEM cell) retrofitted with environmental control, which maintained the system under biological conditions (37 °C, 5% CO_2, 95% RH) for the duration of the exposure. Our study delivered a uniform field to the cellular samples, which allowed an accurate prediction of the energy deposition in terms of SAR distribution across the cell monolayer. We confirmed that significant temperature rise did not occur in our conditions by recording the changes in temperature during exposures and also examining changes in the expression of well-known heat stress genes (Fig. 3 and Supplementary Fig. 2). Collectively, this indicates that the observed effect on DNA methylation and gene expression is not associated with bulk heating of the sample. This data is in line with previous studies that showed biological effects in the absence of significant heat [Velizarov et al., 1999; Yu and Yao 2010; IARC, 2013; Loos et al., 2013; Marjanovic Cermak et al., 2017; Belpomme et al., 2018; Halgamuge et al., 2020; Sharma et al., 2022].

Future Directions—Studies of Temporal Effects of RF-EMF Exposures

DNA methylation is a dynamic process and it remains to be determined if the effects described herein are stable or transient. An indicator that the global epigenetic changes induced by RF-EMFs could potentially be a transient event is that we observe no changes in cell viability at 24 h postexposure (Fig. 1C). Furthermore, the lack of a correlation for all the identified DMGs and DEGs should not undercut the importance of the individual datasets nor the potential for each to be exploited for RF-EMF exposure biomarker identification. The fact that only a few common genes were correlated in our DMG and DEG comparison suggests that DNA methylation is not the underlying mechanism for immediate changes in gene expression observed in our study (which harvested RNA immediately at the end of RF-EMF exposures). This finding was not surprising since it is well-accepted that the relationship between DNA methylation and gene expression is not a perfect cause and effect correlation since gene expression can be controlled by different simultaneous mechanisms. Further, since the analyses were performed only on RNA extracted immediately after exposure, we cannot dismiss that DNA methylation could still play a role in regulating the expression of late (delayed) response gene for which gene expression takes hours to days. Changes in such genes were not captured in the present study since it specifically focused on changes in gene expression occurring within 1 h or less of exposure. We recognize the importance of a more comprehensive and temporal analysis of gene expression and global DNA methylation; therefore, future studies will evaluate the cellular responses to RF-EMFs at different postexposure time-points (hours to days). With such analyses, we possibly could pinpoint RF-EMF transient and any potentially persistent effects on epigenetics and define downstream pathways activated following the RF insult.

In summary, the study described herein showed changes in DNA methylation and gene expression immediately following a single exposure to 900 MHz RF-EMFs at a low dose for 1 h. More studies are needed to determine if these are transient or long-standing alterations in the epigenome. Additionally, future studies should also investigate these effects from shorter and longer single exposures as well as investigate effects from multiple exposures.

ACKNOWLEDGMENTS

This research was supported by funds from the Air Force Office of Scientific Research LRIR (AFOSR-LRIR 19RHCOR071). The authors would also like to thank Ms. Hilda Hall for providing valuable editorial and administrative expertise in the revision of this manuscript. This research was performed while X.G.P. held an NRC Research Associateship award at the Air Force Research Laboratory.

REFERENCES

Antwih DA, Gabbara KM, Lancaster WD, Ruden DM, Zielske SP. 2013. Radiation-induced epigenetic DNA methylation modification of radiation-response pathways. Epigenetics 8(8):839–848.

Belpomme D, Hardell L, Belyaev I, Burgio E, Carpenter DO. 2018. Thermal and non-thermal health effects of low

1521186x, 2023, 3-4, Downloaded from https://onlinelibrary.wiley.com/doi/10.1002/bem.22439 by University Of British Columbia, Wiley Online Library on [10/10/2026]. See the Terms and Conditions (https://onlinelibrary.wiley.com/terms-and-conditions) on Wiley Online Library for rules of use; OA articles are governed by the applicable Creative Commons License

intensity non-ionizing radiation: An international perspective. Environ Pollut 242(Pt A):643–658.
Belyaev IY, Alipov YD, Harms-Ringdahl M. 1997. Effects of zero magnetic field on the conformation of chromatin in human cells. Biochim Biophys Acta (BBA)—General Subjects 1336(3):465–473.
Belyaev IY, Markovà E, Hillert L, Malmgren LOG, Persson BRR. 2009. Microwaves from UMTS/GSM mobile phones induce long-lasting inhibition of 53BP1/γ-H2AX DNA repair foci in human lymphocytes. Bioelectromagnetics 30(2):129–141.
Belyaev IY, Koch CB, Terenius O, Roxström-Lindquist K, Malmgren LOG, Sommer WH, Salford LG, Persson BRR. 2006. Exposure of rat brain to 915 MHz GSM microwaves induces changes in gene expression but not double stranded DNA breaks or effects on chromatin conformation. Bioelectromagnetics 27(4):295–306.
Blattenberger K. 2022. Dielectric constant, strength, & loss tangent—RF cafe. [online] Rfcafe.com. Available from: https://www.rfcafe.com/references/electrical/dielectric-constants-strengths.htm.
Cermak AMM, Pavicic I, Lovakovic BT, Pizent A, Trosic I. 2017. In vitro non-thermal oxidative stress response after 1800 MHz radiofrequency radiation. General Physiol Biophys 36(4):407–414.
Chowdhury AMMA, Katoh H, Hatanaka A, Iwanari H, Nakamura N, Hamakubo T, Natsume T, Waku T, Kobayashi A. 2017. Multiple regulatory mechanisms of the biological function of NRF3 (NFE2L3) control cancer cell proliferation. Sci Rep 7(1):12494.
Churchill SW, Chu HHS. 1975. Correlating equations for laminar and turbulent free convection from a vertical plate. Int J Heat Mass Transfer 18(11):1323–1329.
Crameri F. 2021. Scientific colour maps (7.0.1). Zenodo. https://doi.org/10.5281/zenodo.5501399
Crameri F, Shephard GE, Heron PJ. 2020. The misuse of colour in science communication. Nat Commun 11:5444. https://doi.org/10.1038/s41467-020-19160-7
Dasdag S, Akdag MZ, Erdal ME, Erdal N, Ay OI, Ay ME, Yilmaz SG, Tasdelen B, Yegin K. 2015a. Long term and excessive use of 900 MHz radiofrequency radiation alter microRNA expression in brain. Int J Radiat Biol 91(4):306–311.
Dasdag S, Akdag MZ, Erdal ME, Erdal N, Ay OI, Ay ME, Yilmaz SG, Tasdelen B, Yegin K. 2015b. Effects of 2.4 GHz radiofrequency radiation emitted from Wi-Fi equipment on microRNA expression in brain tissue. Int J Rad Biol 91(7):555–561.
Durney CH, Massoudi H, Iskander MF. 1986. Radiofrequency radiation dosimetry handbook. 4th edition. Final report, 1 July 1984–31 December 1985. United States.
Echchgadda I, Grundt JE, Cerna CZ, Roth CC, Payne JA, Ibey BL, Wilmink GJ. 2016. Terahertz radiation: a non-contact tool for the selective stimulation of biological responses in human cells. IEEE Trans Terahertz Sci Technol 6(1):54–68.
Federal Communications Commission. 2019. Federal communications commission's rules regarding human exposure to radiofrequency electromagnetic fields. 34 FCC Rcd 11687 (14).
Halgamuge MN, Skafidas E, Davis D. 2020. A meta-analysis of in vitro exposures to weak radiofrequency radiation exposure from mobile phones (1990-2015). Environ Res 184:109227.
Hansen KD, Langmead B, Irizarry RA. 2012. BSmooth: from whole genome bisulfite sequencing reads to differentially methylated regions. Genome Biol 13(10):R83.
Heinz S, Benner C, Spann N, Bertolino E, Lin YC, Laslo P, Cheng JX, Murre C, Singh H, Glass CK. 2010. Simple combinations of lineage-determining transcription factors prime cis-regulatory elements required for macrophage and B cell identities. Mol Cell 38(4):576–589.
Hershko A. 2005. The ubiquitin system for protein degradation and some of its roles in the control of the cell-division cycle (Nobel lecture). Angewandte Chemie Int Ed 44(37):5932–5943.
IARC Working Group on the Evaluation of Carcinogenic Risks to Humans. 2013. Non-ionizing radiation, Part 2: Radiofrequency electromagnetic fields. IARC Monogr Eval Carcinog Risks Humans 102(Pt 2):1–460.
Jones PA. 2012. Functions of DNA methylation: islands, start sites, gene bodies and beyond. Nat Rev Genetics 13(7):484–492.
Kalinich JF, Catravas GN, Snyder SL. 1989. The Effect of γ Radiation on DNA Methylation. Radiat Res 117(2):185–197.
Koizumi S, Irie T, Hirayama S, Sakurai Y, Yashiroda H, Naguro I, Ichijo H, Hamazaki J, Murata S. 2016. The aspartyl protease DDI2 activates Nrf1 to compensate for proteasome dysfunction. eLife 5:e18357.
Koturbash I, Pogribny I, Kovalchuk O. 2005. Stable loss of global DNA methylation in the radiation-target tissue--a possible mechanism contributing to radiation carcinogenesis? Biochem Biophys Res Commun 337(2):526–533.
Kovalchuk O, Burke P, Besplug J, Slovack M, Filkowski J, Pogribny I. 2004. Methylation changes in muscle and liver tissues of male and female mice exposed to acute and chronic low-dose X-ray-irradiation. Mutat Res/Fundament Mol Mech Mutagen 548(1-2):75–84.
Kuhmann C, Weichenhan D, Rehli M, Plass C, Schmezer P, Popanda O. 2011. DNA methylation changes in cells regrowing after fractioned ionizing radiation. Radiother Oncol 101(1):116–121.
Kültz D. 2003. Evolution of the cellular stress proteome: from monophyletic origin to ubiquitous function. J Exp Biol 206(Pt 18):3119–3124.
Kültz D. 2005. Molecular and evolutionary basis of the cellular stress response. Ann Rev Physiol 67:225–257.
Liu J, Lin A. 2005. Role of JNK activation in apoptosis: A double-edged sword. Cell Res 15(1):36–42.
Liu J, Minemoto Y, Lin A. 2004. c-Jun N-terminal protein kinase 1 (JNK1), but not JNK2, is essential for tumor necrosis factor alpha-induced c-Jun kinase activation and apoptosis. Mol Cell Biol 24(24):10844–10856.
Loos N, Thuróczy G, Ghosn R, Brenet-Dufour V, Liabeuf S, Selmaoui B, Libert JP, Bach V, Diouf M, de Seze R. 2013. Is the effect of mobile phone radiofrequency waves on human skin perfusion non-thermal? Microcirculation 20(7):629–636.
Ma S, Liu X, Jiao B, Yang Y, Liu X. 2010. Low-dose radiation-induced responses: focusing on epigenetic regulation. Int J Radiat Biol 86(7):517–528.
Mashima R, Hishida Y, Tezuka T, Yamanashi Y. 2009. The roles of Dok family adapters in immunoreceptor signaling. Immunol Rev 232(1):273–285.
Miousse IR, Kutanzi KR, Koturbash I. 2017. Effects of ionizing radiation on DNA methylation: from experimental biology to clinical applications. Int J Radiat Biol 93(5):457–469.
Mokarram P, Sheikhi M, Mortazavi SMJ, Saeb S, Shokrpour N. 2017. Effect of exposure to 900 MHz GSM mobile phone radiofrequency radiation on estrogen receptor methylation status in colon cells of male Sprague Dawley rats. J Biomed Phys Eng 7(1):79–86.

1521186x, 2023, 3-4, Downloaded from https://onlinelibrary.wiley.com/doi/10.1002/bem.22439 by University Of British Columbia, Wiley Online Library on [10/10/2026]. See the Terms and Conditions (https://onlinelibrary.wiley.com/terms-and-conditions) on Wiley Online Library for rules of use; OA articles are governed by the applicable Creative Commons License

Moore LD, Le T, Fan G. 2013. DNA methylation and its basic function. Neuropsychopharmacology 38(1):23–38.
Peyman A, Gabriel C, Grant EH. 2007. Complex permittivity of sodium chloride solutions at microwave frequencies. Bioelectromagnetics 28(4):264–274.
Plongthongkum N, Diep DH, Zhang K. 2014. Advances in the profiling of DNA modifications: Cytosine methylation and beyond. Nat Rev Genetics 15(10):647–661.
Remcom. 2020. XFDTD 7.9 Reference Manual.
Sage C, Burgio E. 2017. Electromagnetic fields, pulsed radiofrequency radiation, and epigenetics: How wireless technologies may affect childhood development. Child Develop 89(1):129–136.
Schuderer J and Kuster N. 2003. Effect of the meniscus at the solid/liquid interface on the SAR distribution in Petri dishes and flasks. Bioelectromagnetics 24:103–108.
Schuderer J, Samaras T, Oesch W, Spat D, Kuster N. 2004. High peak SAR exposure unit with tight exposure and environmental control for in vitro experiments at 1800 MHz. IEEE Trans Microwave Theory Techniques 52(8):2057–2066.
Sharma S, Bahel S, Katnoria JK. 2022. Evaluation of oxidative stress and genotoxicity of 900 MHz electromagnetic radiations using Trigonella foenum-graecum test system. Protoplasma: 1–16.
Shaulian E, Karin M. 2002. AP-1 as a regulator of cell life and death. Nat Cell Biol 4(5):E131–136.
Tawa R, Kimura Y, Komura JI, Miyamura Y, Kurishita A, Sasaki MS, Sakurai H, Ono T. 1998. Effects of X-ray irradiation on genomic DNA methylation levels in mouse tissues. J Radiat Res 39(4):271–278.
Tournier C, Hess P, Yang DD, Xu J, Turner TK, Nimnual A, Bar-Sagi D, Jones SN, Flavell RA, Davis RJ. 2000. Requirement of JNK for stress-induced activation of the cytochrome c-mediated death pathway. Science 288(5467):870–874.
Velizarov S, Raskmark P, Kwee S. 1999. The effects of radiofrequency fields on cell proliferation are non-thermal. Bioelectrochem Bioenerget 48(1):177–180.
Wei LX, Goodman R, Henderson A. 1990. Changes in levels of c-myc and histone H2B following exposure of cells to low-frequency sinusoidal electromagnetic fields: evidence for a window effect. Bioelectromagnetics 11(4):269–272.
Whitfield BL, Billen D. 1972. In vivo methylation of Escherichia coli DNA following ultraviolet and x-irradiation. J Mol Biol 63(3):363–372.
Yu Y, Yao K. 2010. Non-thermal cellular effects of lowpower microwave radiation on the lens and lens epithelial cells. J Int Med Res 38(3):729–736.

SUPPORTING INFORMATION

Additional supporting information may be found online in the Supporting Information section at the end of the article.

1521186x, 2023, 3-4, Downloaded from https://onlinelibrary.wiley.com/doi/10.1002/bem.22439 by University Of British Columbia, Wiley Online Library on [10/10/2026]. See the Terms and Conditions (https://onlinelibrary.wiley.com/terms-and-conditions) on Wiley Online Library for rules of use; OA articles are governed by the applicable Creative Commons License